THEORY AND SIMULATION FOR THE ORIENTATION OF HIGH-ASPECT-RATIO PARTICLES SETTLING IN HOMOGENEOUS ISOTROPIC TURBULENCE

A Thesis

Presented to the Faculty of the Graduate School

of Cornell University

in Partial Fulfillment of the Requirements for the Degree of

Master of Science

by

Udayshankar Menon

August 2019

ABSTRACT

When anisotropic particles settle in isotropic turbulence, the inertial torque due to their settling favors broadside alignment while turbulence favors orientation dispersion. This process leads, for example, to the anisotropic scattering of electromagnetic radiations in icy clouds due to the orientation distribution of ice crystals, which can have needle-like or disk-like shapes. We study two types of particles amenable to the use of slender-body theory (Batchelor 1970, Khayat and Cox 1989): fibers and planar triads consisting of three connected rods. In our approach we use slender-body theory to model these high aspect ratio particles and use stochastic models to describe the fluid flow. For particles smaller than the Kolmogorov scale, the effect of turbulence can be described in terms of a temporally fluctuating local linear flow field following the motion of the particle. When the settling velocity is small compared with the Kolmogorov velocity, the particle samples the fluid velocity gradients along a Lagrangian path, and our simulations employ the stochastic velocity gradient model of Girimaji and Pope (1990). When the settling velocity is large compared with the Kolmogorov velocity, the large inertial torque causes the particle to achieve a quasi-steady orientation with respect to the local velocity gradient allowing analytical predictions of the small orientational dispersion away from the preferred horizontal alignment. Through our simulations and theory, we identify a settling parameter S_F and an asymptotic power-law dependence of orientational variance on the same. We eventually compare our simulation results to experiments and derived theoretical asymptotes.

To all those who suffer(ed) from depression and anxiety in graduate school.

ACKNOWLEDGEMENTS

I would like to thank my advisor Prof. Donald Koch for his continued support over the last couple of years. I am grateful for his advice and suggestions provided during this time. I also extend my appreciation to my colleagues at Koch group and the faculties at Cornell University.

I would like to thank Prof. Anubhab Roy for his continued support with this project and in co-writing our manuscript on this work.

I thank my collaborators at Wesleyan University and Voth group, especially Prof. Greg Voth and Dr. Stefan Kramel, for their insights and experimental results.

I would like to also thank Dr. Vaithianathan Thirunavukkarasu, Dr. Peter Ireland, Prof. Lance Collins, and my colleague Melanie Li Sing How, for their support at various junctures during my pursuit of this project.

I am forever indebted to the Counseling and Psychological Services (CAPS) provided at Cornell Health for their confidential and professional services.

I would like to thank Kevin Kimura, Arunodai Vudem, Maximilian Nguyen, Prajwal Prakash, Pranav Gupta, and Maria Teresa Reinoso Perez for their support and friendship. I would like to also thank my housemates at Stewart Little Co-op for letting me be a part of their lives.

I would like to finally thank Amma, Achan, Nanu and Sriram, for supporting me unconditionally over the years and encouraging me to pursue my passion and dreams.

TABLE OF CONTENTS

LIST OF TABLES

LIST OF FIGURES

CHAPTER 1

INTRODUCTION

Sedimentation of non-spherical particles is of importance in natural and applied processes. In clouds, for example, ice crystals have a planar structure, which leads to preferential alignment and reflection of electromagnetic radiation. Polarization lidar observations have tried to correlate the scattering of light to the angular deviations of these particles from the horizontal [15, 19, 24]. Lidar polarization studies serve as an important tool to study these high altitude clouds and in understanding the influence of sunlight on weather model parameters. In vertical pneumatic gas-solid lines, it was noticed that there is a lack of experimental correlations and computational fluid dynamics models to predict the pressure drop in gas-solid flows containing highly aspherical particles [10]. From an engineering and applied perspective, there is a lack of theoretical studies on the sedimentation of high-aspect ratio particles in turbulence. Unlike spherical particles, high-aspect ratio particles such as fibers, rods and disks, have an orientation dependence to their particle translation and orientation dynamics. There have been simulations of neutrally buoyant particles in homogeneous isotropic turbulence (HIT) [20, 25, 18], and of fibers translating in a fluid [22, 21], however, there have been no Direct Numerical Simulation (DNS) of fibers settling in turbulence that captures the effects of fluid inertia as a two-way coupled interaction between fluid and particles. This is due to the computational difficulty of performing two-way coupled DNS of fibers. Fluid inertia is important in understanding the orientation dynamics of fibers and other high aspect ratio particles, and can be captured in DNS by coupling the particle and fluid dynamics. This would warrant enforcing the particle and fluid forcing for drag and turbulence in the pseudo-spectral simulation. Experimental studies

have also considered the case of small neutrally buoyant aspherical particles in turbulence [16, 14, 9] and has been reviewed by Voth and Soldati [23]. However, at larger particle sizes, the effects of fluid inertia are more profound and cannot be neglected. Most studies on non-spherical particles in turbulence have neglected the effects of torque due to fluid inertia [27, 28, 8]. It has been recognized in atmospheric science literature [5, 15, 12] that inertial torque causes horizontal alignment of ice crystals in cloud turbulence. Inertial torques cause slender particles to sediment with their long axis perpendicular to gravity.

In this work, we propose a settling parameter S_F that determines the relative influence of turbulence and fluid inertia. We then proceed to show the transition of non-spherical particles from isotropic distribution at high turbulence $S_F \ll 1$ to horizontal alignment at high settling rates $S_F \gg 1$. Instead of considering spheroidal particles, we introduce ramified particles to facilitate our theory and simulation approach. Ramified particles are structures capable of capturing different symmetries, formed by connecting fibers or slender rods together. By doing so, we exploit the slender body theory [1] to model fibers and thus these complicated geometries. For example, three fibers connected to form a coplanar structure of equal separation that we refer to as a triad, captures the symmetries of a disk. Similarly, one might form other shapes and structures by connecting fibers and introducing rigid body constraints. Another motivation to study ramified particles is because of the ease in fabricating these structures using 3D printing technology to perform experiments [13]. A primary objective of our simulations and theory is to eventually compare to experimental observations of triads settling in Homogeneous Isotropic Turbulence (HIT). We have in this regard, developed simple models based of slender body theory, capturing the effects of fluid inertia as a torque given by Khayat and Cox [11] for high-aspect

ratio particles. To overcome the computational difficulties of performing DNS of fibers in HIT, a stochastic model of turbulence velocity gradient of Girimaji and Pope [7] is chosen.

In section 2.3 and 2.3.1, a detailed description of the model and assumptions made to facilitate the simulations and theory is discussed. There is a brief discussion of the simulations before extending the same to triads in section 2.4. Finally, the simulations and theory is compared to experimental findings [13] in section 2.5.

CHAPTER 2

THEORY AND RESULTS

2.1 Motivation

Anisotropic particles settle unlike isotropic particles due to their preferred settling orientations. While the settling dynamics of a sphere is determined by its translation velocity, for a fiber, its orientation plays a critical role in determining the direction and rate of settling. This difference is notable for a fiber settling in a quiescent non-inertial flow. In the absence of fluid inertia, like in the case of Stokes flow, $Re_\ell = W\ell/\nu = 0$ where W is the magnitude of particle velocity, $L = 2\ell$ is particle length and ν is the kinematic viscosity of the fluid, the settling trajectory for a fiber is determined by its initial orientation. It is observed that a fiber in Stokes flow has a maximum settling velocity at its vertical orientation, which is twice its minimum velocity observed at a horizontal orientation. This lack of change in orientation or trajectory during settling is attributed to the lack of fluid inertia at these flow regimes. In the presence of fluid inertia however, a fiber tends to achieve a broadside alignment. In other words, it may be noted that the horizontal orientation of settling is the only stable orientation of settling for a fiber in the presence of fluid inertia. This broadside alignment is due to the presence of an inertial torque that is a result of particle orientation and settling velocity. Khayat and Cox [11] have determined the leading order contribution to this torque at the limit of weak fluid inertia, $Re_\ell \ll 1$. The objective of this work is to provide a theoretical framework to tackle orientation dynamics of fibers and other anisotropic particle settling in turbulence.

It is to be expected, that this competition of inertial and turbulent torque will

result in an orientation distribution for such particles. In clouds, ice crystals tend to achieve orientations that influence the reflection of electromagnetic radiations. An ice crystal has a planar hexagonal shape and symmetries similar to a disk. Sunlight is the primary source of energy to Earth and serves as an important parameter in weather models. Understanding the orientation of ice crystals in clouds would help determine the fraction of light that enters the atmosphere. The reflection of electromagnetic radiations is also of motivation to airplanes to develop better navigation and frost prediction techniques.

In this section, simple particle models for fibers and geometries that capture disk-like symmetries are developed. These models are then coupled to Lagrangian stochastic models of turbulence [7, 17, 4, 3] to simulate the particle orientation distributions. By assuming the limit of weak fluid inertia, $Re_\ell \ll 1$, one may exploit the inertial torques at leading order of Khayat and Cox to capture the effects of fluid inertia. It is expected that the fiber experiences two primary contributions to its orientation dynamics, a randomization due to the stochastic turbulent velocity field and a broadside alignment due to fluid inertia. Through the sections ahead, we provide simulations and analytic results supporting this claim, and also derive parameters that help in describing the orientation distribution quantitatively.

2.2 Lagrangian model of turbulence

Before we delve into the particle models and scaling arguments, it is important to describe the motivation for selecting the turbulence model we have in this work. As mentioned, the objective of this work has been to develop simple particle models that are able to describe the salient features responsible for the

interesting orientation distributions. To provide a complete description of the orientation distribution of these high-aspect ratio particles such as fibers and rods, one must solve the entire fluid flow equations. In other words, a Direct Numerical Simulation (DNS) in the presence of particles must be solved. This is a rather exhaustive process considering the computational expense and difficulty involved. There is a lack of easy to use, open source DNS solvers that are easy to implement and modify. Also, inertial torque experienced by fibers is a result of two-way coupled dynamics. Capturing such effects is rather complicated and yet to be successfully implemented in the presence of turbulence. Previous studies have, therefore, either ignored turbulence or fluid inertia to simulate the orientation dynamics of fibers [20, 21, 22]. To overcome this difficulty but at the same time to provide a framework to understand the orientation distribution of fibers, we have chosen stochastic models of turbulence to provide a temporal distribution of the flow field. In this regard, there are different models of turbulence available, but in this work a Lagrangian stochastic model of homogeneous, isotropic turbulence of Girimaji and Pope [7] was chosen. This model provides a temporal distribution of velocity gradient capturing the non-linear terms of Navier -Stokes equation exactly and has parameters, such as the pseudo-dissipation, relaxation time of pseudo-dissipation and strain rate, and moments of velocity gradient, tuned to imitate the DNS findings of Yeung and Pope [26]. High-aspect ratio particle dynamics is dependent on the correlation of vorticity and shear, and this model does a good job of capturing it, making it suitable for our objective of simulating the orientation distribution of fibers. By approximating the fibers to be sub-Kolmogorov, it may be assumed that the particle experiences a local stochastic linear flow field in turbulence. At slow settling rates, it is fair to assume that particle follows fluid trajectory, justifying

the choice of a Lagrangian model of turbulence.

As already mentioned, Girimaji and Pope [7] model the non-linear terms in Navier Stokes equation exactly, and capture the correlation of vorticity and shear quite well. The model is based on the log-normal distribution of pseudo-dissipation observed in DNS of Yeung and Pope [26]. Chen and Pope [17] have modeled pseudo-dissipation as a Uhlenbeck-Ornstein process of diffusion. This model has been further extended to obtain a stochastic equation of velocity gradient. The simulation generates a temporal distribution of velocity gradient by solving diffusion equations of pseudo-dissipation ϕ and velocity gradient Γ_{ij} simultaneously.

$$d\phi = \phi dt\left(\hat{a}^2 - \frac{\ln\phi}{\tau}\right) + (2\hat{a}\phi)\, dW \tag{2.1}$$

$$d\Gamma_{ij} = -N_{ij}dt - \Gamma_{ij}\left(\frac{7}{2}\hat{a}^2 + \frac{\ln\phi}{2\tau} - \frac{\Gamma_{lm}N_{lm}}{\phi}\right)dt + L_{ij}dt + D_{ijkl}dW_{kl} \tag{2.2}$$

where $\hat{a}^2$ is the normalized variance, τ is the ratio between integral time scale and Kolmogorov time scale, dW and dW_{kl} are the scalar and tensor Wiener process increments. The other terms in 2.2 such as N_{ij}, L_{ij} and D_{ijkl} hold the same definitions as in the original paper of Girimaji and Pope [7].

2.3 Small fibers settling in turbulence

The idea of simulating small enough fibers is motivated from the fact that we intend to use Lagrangian stochastic models of velocity gradient to describe turbulence. For a small enough particle of sub-Kolmogorov length scales ($L \ll \eta$), the fiber experiences a local linear flow field. In a homogeneous isotropic turbulent flow, this would be a randomly varying isotropic flow field. In the absence of any fluid inertia, a particle would align in the direction of minimum

shear, giving an isotropic distribution of orientation [20]. However, fluid inertia breaks this degeneracy and aligns the particle horizontally, creating a distribution of orientation due to competing effects. This competition of preferential alignment and randomization of orientation can be understood in terms of two time scales. There is a time scale over which the particle responds to the eddies of turbulence ($O(\tau_L)$) and another for response to fluid inertia that we shall define as τ_{sed}. A particle of length L would respond primarily to an eddy of similar size, and "filters" any eddy smaller than this. Depending on the rate of settling and turbulence intensity (Re_λ), we can then argue the relative influence of these two effects. A settling parameter S_F is then defined as the ratio of these two time scales to parameterize the domain over which one may study the orientation distribution.

$$S_F \equiv \frac{\tau_L}{\tau_{sed}} \tag{2.3}$$

For a sub-Kolmogorov particle, this eddy turn over time would correspond to the Kolmogorov scale of turbulence. A heuristic definition of the time scale over which a particle responds to inertial torque, τ_{sed} is obtained as the inverse rotation rate of a particle at $\theta = 45^\circ$ in the absence of turbulence. The angle θ is defined as that between the axis of symmetry and gravity, for a fiber it is the angle between the orientation vector and gravity, for a disk or triad it is the angle between the normal to plane of particle and gravity. A practical definition of S_F for sub-Kolmogorov particles is then obtained as,

$$S_F = \frac{\tau_\eta}{\tau_{sed,45^\circ}} \tag{2.4}$$

A settling particle of length $L = 2\ell$ disturbs a fluid volume of $O(L^3)$. Upon

comparing the particle and fluid masses that are disturbed, one obtains,

$$\frac{\rho_p}{\rho_f} \ll \left(\frac{L}{D}\right)^2 = \kappa^2 \tag{2.5}$$

From this relation it may be noticed that for high aspect ratio particles, whenever the particle and fluid densities are comparable, the particle inertia is negligible compared to that of the fluid. This allows one to neglect particle inertia and assume that the particle experiences no net force or torque. Any external force must be then balanced by drag and lift forces generated due to relative velocity between particle and fluid phases. Batchelor [1] derived analytic expressions for the drag and lift force, valid at $Re_\ell \ll 1$ and $\kappa \gg 1$. The balance of forces expressed at leading order in κ and low Re_ℓ is then,

$$\frac{4\pi\mu L}{\ln(2\kappa)}\left(\boldsymbol{I} - \frac{1}{2}\boldsymbol{pp}\right)\cdot\mathbf{W} - m\mathbf{g} = 0, \tag{2.6}$$

where $\boldsymbol{I}$ is the identity matrix, $m = (\rho_p - \rho_f)\pi LD^2/4$ is the mass difference between a cylindrical fiber and the displaced fluid, μ is the dynamic fluid viscosity and $\mathbf{g}$ is gravity. A fiber will therefore translate with a quasi-steady state velocity $\mathbf{W}$ relative to the local fluid velocity. Equation 2.6 yields the well-known relationship between the transverse and longitudinal settling velocities of a fiber

$$W_{max} = 2W_{min} \tag{2.7}$$

where $W_{max} = |\boldsymbol{W}|_{\theta=0}$ and $W_{min} = |\boldsymbol{W}|_{\theta=\pi/2}$, respectively. Here, θ is the angle between $\boldsymbol{p}$ and gravity $\hat{\boldsymbol{e}}_{\boldsymbol{g}}$.

While one can neglect particle inertia effects on the settling velocity of small fibers, fluid inertia is necessary to break the degeneracy of particle orientation when a particle settles in a quiescent fluid. With the inclusion of fluid inertia, fibers experience inertial torques $\boldsymbol{G}_{sed}$ that rotate the particle to an equilibrium orientation where $\boldsymbol{p}$ is perpendicular to $\boldsymbol{W}$, and for most part to gravity. Khayat

and Cox [11] derived expressions for torque experienced by a translating fiber $\boldsymbol{G}_{sed}$, in the low Reynolds number limit ($Re_\ell \ll 1$) and leading order in high aspect ratio κ as

$$\boldsymbol{G}_{sed} = \frac{5\pi\rho_f L^3}{24(\ln 2\kappa)^2}(\boldsymbol{W}\cdot\boldsymbol{p})(\boldsymbol{W}\times\boldsymbol{p}) \tag{2.8}$$

This $O(Re_\ell)$ inertial torque breaks the degeneracy of particle orientation and leads to broadside alignment.

The particle also experiences a rotational resistance $\boldsymbol{G}_{rel}$ to its relative rotation [1]:

$$\boldsymbol{G}_{rel} = \frac{\pi\mu L^3}{3\ln(2\kappa)}\boldsymbol{\Omega}_{rel} \tag{2.9}$$

Here, $\boldsymbol{\Omega}_{rel}$ is the relative rotation of the particle with respect to the local fluid rotation. In addition, fibers experience torque due to the fluid strain rate $\boldsymbol{S} = \frac{1}{2}(\boldsymbol{\Gamma}+\boldsymbol{\Gamma}^T)$:

$$\boldsymbol{G}_{strain} = \frac{\pi\mu L^3}{3\ln(2\kappa)}(\boldsymbol{p}\times(\boldsymbol{S}\cdot\boldsymbol{p})) \tag{2.10}$$

Here, $\boldsymbol{\Gamma}$ is the turbulent velocity gradient.

For a symmetric fiber sedimenting in turbulence, in the absence of particle inertia, a torque balance then reads as,

$$\underbrace{\frac{5\pi\rho_f L^3}{24(\ln 2\kappa)^2}(\boldsymbol{W}\cdot\boldsymbol{p})(\boldsymbol{W}\times\boldsymbol{p})}_{inertial\ \ sedimentation} + \underbrace{\frac{\pi\mu L^3}{3\ln(2\kappa)}\boldsymbol{\Omega}_{rel}}_{relative\ \ rotation} + \underbrace{\frac{\pi\mu L^3}{3\ln(2\kappa)}(\boldsymbol{p}\times(\boldsymbol{S}\cdot\boldsymbol{p}))}_{turbulent\ \ strain} = 0 \tag{2.11}$$

The zero torque balance yields the following equation for the rate of change of fiber orientation, $\dot{\boldsymbol{p}}$ as,

$$\dot{\boldsymbol{p}} = \boldsymbol{p}.\boldsymbol{\Gamma} - \boldsymbol{p}\,(\boldsymbol{p}.\boldsymbol{S}.\boldsymbol{p}) + \frac{5}{8\nu\ln(2\kappa)}(\boldsymbol{W}\cdot\boldsymbol{p})\ \boldsymbol{W}\cdot(\boldsymbol{pp}-\boldsymbol{I}) \tag{2.12}$$

where the first two terms correspond to Jeffery rotation in the local linear flow field and the last term is the rotation due to the inertial torque caused by the particles sedimentation. An alternative form of the tumbling rate due to inertial

torque is

$$\dot{\boldsymbol{p}}_{\boldsymbol{sed}} = \frac{5}{8\nu \ln(2\kappa)} (\boldsymbol{W}\cdot\boldsymbol{p})(\boldsymbol{W}\times\boldsymbol{p}) \tag{2.13}$$

By coupling the particle model described by equations 2.6 and 2.12, with the turbulence model in previous section, a temporal simulation for the translation and rotation dynamics of small fibers is generated. We have performed these simulations for $Re_\lambda = 38,\ 93$ and for a range of minimum horizontal velocities W_{min}.

As already mentioned, $\tau_{sed,45^\circ}$ is defined as the time scale of response to fluid inertial torque. Theoretically, this may be defined as the inverse of instantaneous particle rotation rate for a fiber oriented at $\theta = 45^\circ$. For a fiber, $\tau_{sed,45^\circ}$ is then obtained analytically by solving the fiber dynamics equations 2.6 and 2.13, at $\theta = 45^\circ$ as

$$\tau_{sed,45^\circ} = \frac{1}{|\dot{\boldsymbol{p}}_{sed,45^\circ}|} \tag{2.14}$$

$$|\dot{\boldsymbol{p}}_{sed,45^\circ}| = \frac{5W_{min}^2}{8\nu \ln 2\kappa} \tag{2.15}$$

The theory and simulations we derived and performed assumes $\kappa = 20$, a large-enough aspect ratio to exploit the slender-body theory. At this limit, we then have a settling parameter for fiber S_F^f defined as,

$$S_F^f = \frac{5W_{min}^2}{8\nu \ln 2\kappa\, \Gamma_\eta} \tag{2.16}$$

$$S_F^f = 0.625\, \frac{W_{min}^2}{\nu \ln 2\kappa\, \Gamma_\eta} \tag{2.17}$$

where $W_{min} = \frac{mg \ln 2\kappa}{4\pi\mu L}$ is the minimum velocity of settling for a fiber achieved at horizontal orientation.

Orientation distribution is measured through an order parameter called the orientation variance. This parameter corresponds to the variance of the orientation component in the direction of gravity. For a fiber of orientation $\boldsymbol{p}$, the order parameter is $\langle p_3^2 \rangle$ and it measures the average deviation of the fiber away from

horizontal. In Fig. 2.1, the simulation results are provided for simulation performed at $Re_\lambda = 38$ and varying minimum velocities. As may be observed, there is a change in the order parameter from a constant value at low S_F to an asymptotic limit at higher S_F.

When $S_F \ll 1$, the particle responds quickly to the Kolmogorov time scale or turbulence. As a result, the fiber tends to align in an isotropic manner due to the stochastic nature of isotropic turbulence. This isotropic orientation distribution is seen in our Lagrangian stochastic simulation, where it is fair to assume that the particle follows a fluid trajectory considering the low settling velocities at $S_F \ll 1$. This constant asymptote at low S_F, corresponds to the isotropic distribution and $\langle p_3^2 \rangle = 0.33$. However, as one increases the settling velocity W_{min}, the particle tends to align horizontally due to the increasing inertial torque. It is important to remember that the simulations assume weak fluid inertia $Re_\ell \ll 1$. This broadside alignment appears as a decrease in the orientation variance, eventually reaching an asymptotic limit at $S_F \gg 1$. It is shown ahead that the fiber at this rapid settling limit has S_F^{-2} behaviour. The fiber orientation at this limit may be described as almost horizontal with a slight "wiggle".

2.3.1 Rapid settling limit of small fibers

In this subsection, an analytic prediction for the variance of the orientation in the rapid settling limit, $S_F = \tau_\eta/\tau_{sed} \gg 1$ is presented. This indicates that the relaxation of fiber orientation toward its equilibrium horizontal alignment occurs much more rapidly than the Kolmogorov time scale. It can be seen that this limit corresponds to one in which the time $\tau_{samp} = \eta/W$ for a fiber to sample a Kolmogorov scale eddy is much smaller than τ_η.

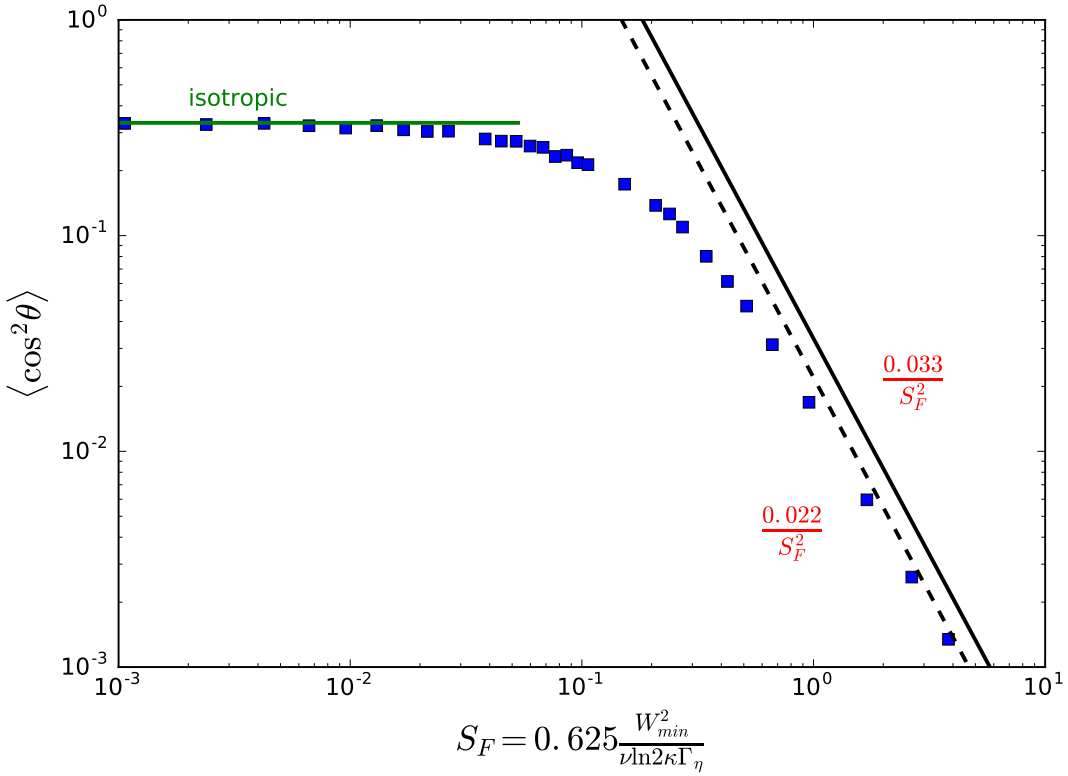

Figure 2.1: Orientation variance of small fibers as a function of settling factor S_F. The squares correspond to simulations and the lines are asymptotes derived in the low and high S_F limits. The solid line at high S_F is obtained by assuming the complete decorrelation of particle orientation and velocity gradient, while the dashed line is asymptote modified to capture their correlation as observed in simulation. The annotated equations correspond to the asymptotes.

In particular, $\tau_\eta/\tau_{samp} = W/u_\eta = S_F^{1/2}[\ln(2\kappa)]^{1/2} \gg 1$. From these it can be argued that the relaxation of fiber orientation is much faster than the sampling time,

$$\frac{\tau_{sed}}{\tau_{samp}} = \frac{[\ln(2\kappa)]^{1/2}}{S_F^{1/2}} \ll 1 \tag{2.18}$$

Thus we have,

$$\tau_{sed} \ll \tau_{samp} \ll \tau_{\eta} \tag{2.19}$$

Even at the high sampling rate, we see that the fiber responds to inertial torque quickly and therefore remains in a horizontal orientation, allowing for the fiber orientation to be analytically obtained from a quasi-steady state balance of inertial rotation and turbulent shear. It should be also noted that τ_{sed} is a response to the inertial torque due to settling and is of consequence only in that direction. As a result, the quasi-steady for fibers would exist in the direction of settling that we have chosen to be 3-direction in our analysis.

We then proceed to determine the rotation rate of fibers whose orientations exhibit small deviations from the horizontal plane, so that $\langle {p_3}^2 \rangle \ll 1$ where the 3-axis is parallel to gravity. We begin with an alternate mobility form of Eq. 2.6 written using Einstein notation,

$$W_i = \frac{mg \ln 2\kappa}{4\pi\mu L} \left(\delta_{ij} + p_i p_j\right) \delta_{j3} = \frac{mg \ln 2\kappa}{4\pi\mu L} \left(\delta_{i3} + p_i p_3\right) \tag{2.20}$$

where $W_{min} = \frac{mg \ln 2\kappa}{4\pi\mu L}$. For $\langle {p_3}^2 \rangle \ll 1$, it can be seen that

$$W_i p_i = 2W_3 p_3 = \frac{mg \ln 2\kappa}{8\pi\mu l} p_3 = 2W_{min} p_3 \tag{2.21}$$

where $W_3 = W_{min}$. Substituting this result into Eq. 2.12 yields,

$$\dot{p}_i = \frac{5}{8\nu \ln 2\kappa} \left(2W_{min} p_3\right) \left(2W_{min} p_3 p_i - W_i\right) + \Gamma_{ij} p_j - p_i S_{lm} p_m p_l \tag{2.22}$$

Since the particle is close to horizontal on an average at this limit, as expected from both theory and simulation, we have $p_3 \ll p_{1,2}$. Thus,

$$\dot{p}_i^t = \Gamma_{ij} p_j^t - p_i^t S_{jl} p_j^t p_l^t \tag{2.23}$$

where p_i^t denotes the transverse component ($i = 1, 2$) of the orientation vector, indicating that the fiber orientation samples the plane normal to gravity by

turbulent shearing motions. This will lead to an isotropic distribution of orientation within the 1,2-plane. Since $\tau_{sed} \ll \tau_\eta$, the motion within the 1,2-plane will be slow compared to the equilibration of the 3-component of fiber orientation. In the settling direction, therefore will exist a quasi-static equilibrium because $\tau_{sed} \ll \tau_{samp}$. Thus,

$$\dot{p}_3 = \frac{20W_{min}^2 p_3}{8\nu \ln 2\kappa} p_3 p_3 - \frac{10W_{min}^2}{8\nu \ln 2\kappa} p_3 + \delta_{i3}\Gamma_{ij}p_j^t - p_3 S_{jl}p_j^t p_l^t = 0 \tag{2.24}$$

Since $p_3 \ll 1$ we further simplify the above equation by balancing the second and third terms to obtain,

$$p_3 \sim \frac{8\nu \ln 2\kappa}{10W_{min}^2}\delta_{i3}\Gamma_{ij}p_j^t \tag{2.25}$$

Thus, the variance characterizing the "wiggle" out of the horizontal plane is

$$\langle p_3^2 \rangle = \left(\frac{8\nu \ln 2\kappa}{10W_{min}^2}\right)^2 \delta_{i3}\delta_{m3}\langle p_j^t p_n^t \rangle \langle \Gamma_{ij}\Gamma_{mn} \rangle = \left(\frac{8\nu \ln 2\kappa}{10W_{min}^2}\right)^2 \delta_{i3}\delta_{m3}\langle p_j^t p_n^t \rangle \left[\langle S_{ij}S_{mn}\rangle + \langle \Omega_{ij}\Omega_{mn}\rangle\right] \tag{2.26}$$

where the $\langle\rangle$ denotes ensemble averages and Ω_{ij} is the anti-symmetric part of the velocity gradient. Cross terms such as $\langle S_{ij}\Omega_{mn}\rangle$ are zero due to isotropy of the turbulent field. In the above expression, we have assumed $\langle p_j^t p_n^t \Gamma_{3j}\Gamma_{3n}\rangle$ to be the corresponding product of mean of velocity gradient $\langle \Gamma_{3j}\Gamma_{3n}\rangle$ and orientation $\langle p_j^t p_n^t\rangle$ dyads. This is a largely valid assumption in the rapid settling limit as $\tau_{sed} \ll \tau_{samp} \ll \tau_\eta$, and as a result, $\boldsymbol{p}^t$ responds to a smaller time scale than the velocity gradient. However, it will be shown soon that this assumption is only true for the component in the direction of gravity. $\langle S_{ij}S_{mn}\rangle$ and $\langle \Omega_{ij}\Omega_{mn}\rangle$ are fourth order isotropic tensors whose form can deduced using the properties of symmetry and continuity, as shown in [2] to obtain

$$\langle S_{ij}S_{mn}\rangle = \frac{S^2}{10}\left[\delta_{im}\delta_{jn} + \delta_{in}\delta_{jm} - \frac{2}{3}\delta_{ij}\delta_{mn}\right] \tag{2.27}$$

$$\langle \Omega_{ij}\Omega_{mn}\rangle = \frac{\Omega^2}{6}\left[\delta_{im}\delta_{jn} - \delta_{in}\delta_{jm}\right] \tag{2.28}$$

where $S^2 = \langle S_{ij} S_{ij} \rangle$ and $\Omega^2 = \langle \Omega_{ij} \Omega_{ij} \rangle$. Substituting Eq. 2.28 in Eq. 2.26 we have

$$\langle p_3^2 \rangle = \left(\frac{8\nu \ln 2\kappa}{10 W_{min}^2} \right)^2 \delta_{i3} \delta_{m3} \left[\frac{S^2}{10} \left(\delta_{im} + \frac{\langle p_i p_m \rangle}{3} \right) + \frac{\Omega^2}{6} \left(\delta_{im} - \langle p_i p_m \rangle \right) \right] = \left(\frac{8\nu \ln 2\kappa}{10 W_{min}^2} \right)^2 \left[\frac{S^2}{10} + \frac{\Omega^2}{6} \right] \tag{2.29}$$

$$\langle p_3^2 \rangle = \left(\frac{8\nu \ln 2\kappa}{10 W_{min}^2} \right)^2 \frac{2\Gamma_\eta^2}{15} = \frac{1}{30} {S_F^f}^{-2} \tag{2.30}$$

where we have used the relations $S^2 = \Omega^2 = \Gamma_\eta^2 / 2$ for homogeneous isotropic turbulence and definition of S_F^f from earlier. Thus, we have for the rapid settling limit the following relation characterizing the departure of orientation from the horizontal plane due to turbulence,

$$\langle p_3^2 \rangle = \langle \cos^2 \theta \rangle = \frac{1}{30} {S_F^f}^{-2} \tag{2.31}$$

However, in our simulations we use a Lagrangian model of velocity gradient instead of a particle frame model of turbulence. At the rapid settling limit, while the strong inertial torque tries to maintain a horizontal orientation, within the 1,2-plane the fiber orientation continues to change at a Kolmogorov time scale. This leads to a correlation of fiber orientation and velocity gradient in horizontal plane. As a result, our simulations give asymptotes different from Eq. 2.31 by a factor corresponding to $\langle p_i^t p_j^t \Gamma_{3i} \Gamma_{3j} \rangle / \left(2\Gamma_\eta^2 / 15 \right)$. In our simulations, we observe this factor to be around 0.66 making the asymptote,

$$\langle \cos^2 \theta \rangle = \frac{0.66}{30} {S_F}^{f\ -2} = 0.022 {S_F^f}^{-2} \tag{2.32}$$

In Fig. 2.1, we compare our simulations to the original theoretical asymptote of Eq. 2.31 and to the corrected relation in Eq. 2.32. Considering the agreement of theory and simulation, it is important to recognize the validity and utility of our assumptions.

2.4 Triads settling in turbulence

In this section, the theory and simulation are extended to triads, 3-armed ramified particles such that all three fiber arms lie within the same plane and at equal separation. We model ramified particles as structures formed of fibers connected together to undergo rigid body dynamics. Thus, by treating the triad as three fibers joined together, the force and torque balances on the triad are:

$$\sum_{n=1}^{3}\left[F^n_{drag}+F^n_{gravity}\right]=\sum_{n=1}^{3}\left[\frac{4\pi\mu L}{\ln(2\kappa)}\left(\mathbb{1}-\frac{1}{2}\boldsymbol{p}'_n\boldsymbol{p}'_n\right)\cdot\boldsymbol{W}_n-m_n\boldsymbol{g}\right]=0 \tag{2.33}$$

$$\sum_{n=1}^{3}\left[\frac{5\pi\rho_f L^3}{24(\ln 2\kappa)^2}(\boldsymbol{W}_n\cdot\boldsymbol{p}'_n)(\boldsymbol{W}_n\times\boldsymbol{p}'_n)-\frac{\pi\mu L^3}{3\ln(2\kappa)}(\mathbb{1}-\boldsymbol{p}'_n\boldsymbol{p}'_n)\cdot\boldsymbol{\Omega}_{rel}+\frac{\pi\mu L^3}{3\ln(2\kappa)}(\boldsymbol{p}'_n\times(\boldsymbol{S}\cdot\boldsymbol{p}'_n))+\ell\boldsymbol{p}'_n\times F^n_{drag}\right]=0 \tag{2.34}$$

where $L=2\ell$ is the arm length. Note that Eq. 2.34 for triads has an additional contribution due to the drag on individual arms, $\boldsymbol{F}^n_{drag}=\frac{4\pi\mu L}{\ln(2\kappa)}\left(\mathbb{1}-\frac{1}{2}\boldsymbol{p}'_n\boldsymbol{p}'_n\right)\cdot\boldsymbol{W}_n$, compared to the torque balance of fibers in Eq. 2.11. From the symmetry of the particle, it may be shown that the contributions to torque due to drag from triad velocity $\boldsymbol{W}_c$, sums to zero. And as a result, only relative velocity of arms with respect to triad center contributes to the torque balance. The orientation of each arm is defined by $\boldsymbol{p}'_n$ and the orientation of a ramified particle is defined by $\boldsymbol{p}$, which is perpendicular to the plane spanned by the arms and is the unit vector along the axis of symmetry. In the low Reynolds number limit, this ramified particle model predicts the same ratio of sedimentation velocities for triads as is known to apply to thin disks (e.g. [6]):

$$W^d_{max}=1.5W^d_{min} \tag{2.35}$$

Since the definition of $\boldsymbol{p}$ is different for triads than for fibers, the definition of W_{max} and W_{min} has also changed, and now $W^d_{max}=|\boldsymbol{W}|_{\theta=\pi/2}$ and $W^d_{min}=|\boldsymbol{W}|_{\theta=0}$.

Note the difference in θ for fibers and disks in Eq. 2.7 and Eq. 2.35. This model neglects hydrodynamic interactions among the rods. The influence of hydrodynamic interactions on the drag and the torque due to relative rotation and straining motions are of higher order in $1/\ln(2\kappa)$. However, hydrodynamic interactions would influence the inertial torque at the same order of magnitude as the terms retained and the present model that includes only the torque on each arm acting independently is likely an underestimate of the triad inertial torque. As a result, upon solving Eq. 2.33 for a horizontal triad, we notice that the minimum velocity of a triad is the same as that of a horizontal fiber. In an actual triad, the arm interactions would appear as fluid inertia effects, and cannot be captured in our simple model, this would require DNS, at the least. When comparing with experimental measurements, the inertial term based on the observed rotation rate of a large triad will correct for this discrepancy. To avoid confusion, though the triad minimum velocity W_{min} is the same as that for a fiber, we will be referring to the latter as W^f_{min}.

It is important to note that our theory applies to a case where the Reynolds number is small $Re_\ell \ll 1$. In this limit, the rotation of the triad toward horizontal orientations is a result of weak fluid inertia. The competition between turbulent shear and inertial rotation leads to intermediate orientation distributions between isotropic and broadside alignment, when $G = \ell\Gamma_\eta/W^f_{min} \ll 1$ and $Re_\ell \ll 1$, but the settling parameter $S^f_F = \frac{5}{8}\left(\frac{Re_\ell}{G}\right) = O(1)$. In order to ensure these conditions in our simulations, especially at higher settling rates ($S_F \gg 1$), we scale our force and torque balance equations. This approach of scaling is necessary to ensure that our simulations agree with the assumptions we have made. We scale Eq. 2.33 using $\mu W^f_{min}\ell^2$ and Eq. 2.34 using $\mu\ell^3\Gamma_\eta$ and express Eq. 2.4 with $\boldsymbol{W}_n = \boldsymbol{W}^c + \boldsymbol{w}_n$, where $\boldsymbol{W}^c$ is the velocity of triad center of mass and $\boldsymbol{w}_n \propto \ell\Gamma_\eta$ is the

disturbance velocity experienced by arms $n = 1, 2, 3$. In the limit of $Re_\ell \ll 1$ and $G = \ell\Gamma_\eta / W^f_{min} \ll 1$, the triad equations reduce to

$$\sum_{n=1}^{3} \left[\left(\mathbb{1} - \frac{1}{2} \boldsymbol{p}'_n \boldsymbol{p}'_n \right) \cdot \bar{\boldsymbol{W}}^c - \hat{\boldsymbol{e}}_g \right] = 0 \tag{2.36}$$

$$\sum_{n=1}^{3} \left[2S^f_F \left(\bar{\boldsymbol{W}}^c \cdot \boldsymbol{p}'_n \right) \left(\bar{\boldsymbol{W}}^c \times \boldsymbol{p}'_n \right) - (\mathbb{1} - \boldsymbol{p}'_n \boldsymbol{p}'_n) \cdot \bar{\boldsymbol{\Omega}}^c + (\boldsymbol{p}'_n \times (\bar{\boldsymbol{S}} \cdot \boldsymbol{p}'_n)) + (\boldsymbol{p}'_n \times (\bar{\boldsymbol{\Gamma}} \cdot \boldsymbol{p}'_n)) \right] = 0 \tag{2.37}$$

where in 2.36, $W^f_{min} = \frac{mg \ln 2\kappa}{4\pi\mu L}$ is transverse velocity of a settling fiber, S^f_F is the settling parameter for fibers defined in Eq. 2.16, $\bar{\boldsymbol{W}}^c = \frac{\boldsymbol{W}^c}{W^f_{min}}$ and $\hat{\boldsymbol{e}}_g$ is the gravitational unit vector. We refer the settling parameter in Eq. 2.37 as S^f_F since it is the same as the definition used for fibers. We will later define an empirical settling parameter S^{emp}_F based of triad rotation rate at $\theta = 45°$. In 2.37, $\bar{\boldsymbol{\Omega}}^c = \frac{\boldsymbol{\Omega}^c}{\Gamma_\eta}$, $\bar{\boldsymbol{S}} = \frac{\boldsymbol{S}}{\Gamma_\eta}$ and $\bar{\boldsymbol{\Gamma}} = \frac{\boldsymbol{\Gamma}}{\Gamma_\eta}$.

The background flow effects in Eq. 2.4 become negligible upon scaling in 2.37 when $Re_\ell \ll 1$ and $G \ll 1$. By an analysis equivalent to that in section 2.3.1, an asymptotic expression for the variance of θ, the angle between normal to plane of triad and the direction of gravity, is obtained. The analysis involves a similar argument where the triad is approximated to be in a quasi-steady horizontal orientation, allowing the angular velocity that would rotate the triad out of 12-plane to be neglected. The asymptotic expression for a triad is qualitatively similar to that of a fiber, with a power law dependence, however, we see a difference of coefficient in Eq. 2.38.

$$\langle \sin^2 \theta \rangle \approx \langle \theta^2 \rangle = \frac{12}{5} S^{f\,-2}_F \tag{2.38}$$

We do not see any correlation of the orientation vector and velocity gradient for triads unlike in fibers, because the normal to the plane of the particle would align vertically or along gravity at rapid settling limit. This behavior is expected to appear for any disk-like symmetric ramified structure. Unlike the fiber ori-

entation rate that had two time sales associated with it depending on the component, the normal to triad and disks align vertically due to the strong inertial torque.

To maintain, uniformity in our definition of S_F, we revert to the empirical definition from previous section. We had defined S_F as the the ratio of time scales of response to turbulence and the inertial torque. By doing so, we obtain an empirical settling parameter for triads as,

$$S_F^t = \frac{\tau_\eta}{\tau_{sed,45^\circ}} \tag{2.39}$$

While for the sub-Kolmogorov triads, like those in simulations, the response time to turbulence remains the Kolmogorov time scale, the time scale of response to inertial torque for triads cannot be easily determined analytically. This is because, unlike the rotation rate of a fiber at $\theta = 45^\circ$, a triad at $\theta = 45^\circ$ has multiple states due to individual arm orientations. Thus, to determine a time scale of response to inertial torque that is independent of the arm orientations within the plane or the angle ψ between arm projection to 12 plane and 1 axis, we need to calculate the reciprocal of an average $\dot{\boldsymbol{p}}_{sed,45^\circ}$. Thus,

$$\tau_{sed,45^\circ} = \frac{1}{\langle|\dot{\boldsymbol{p}}_{sed,45^\circ}|\rangle} \tag{2.40}$$

An analytic integration within a plane at 45° to gravity is cumbersome and to avoid that, we have calculated an average rotation rate within that plane using simulations. We thus have an inertial time scale of response

$$\tau_{sed,45^\circ} \approx 9.48\frac{\nu \ln 2\kappa}{W_{min}^2} \tag{2.41}$$

giving thus, a settling parameter

$$S_F^t \approx 0.105\frac{W_{min}^2}{\nu \ln 2\kappa\, \Gamma_\eta} \tag{2.42}$$

It would be convenient to reduce the theoretical asymptote in Eq. 2.38 to functions of the empirical settling parameter S_F^t. In order to do so, we determine the ratio of the two settling parameters to obtain,

$$\frac{S_F^f}{S_F^t} \approx 5.95 \tag{2.43}$$

Substituting the above expression for S_F^f into the theoretical asymptote of Eq. 2.38,

$$\langle \sin^2\theta \rangle \approx \langle \theta^2 \rangle \approx 0.07\, {S_F^t}^{-2} \tag{2.44}$$

where S_F^t is the empirical settling parameter for triads, based on the average inverse rotation rate at $\theta = 45^\circ$ and Kolmogorov strain rate. In Fig. 2.2, we plot the average variance of the deviation of arms of triad from the horizontal, the order parameter as $0.50\left(1-\theta^2\right)$.

Before comparing the simulations and theory to experimental results, it is important to note that the simulations were carried out at two different turbulence intensities $Re_\lambda = 38,\ 93$. Using the empirical definition of S_F based on inverse rotation rate at $\theta = 45^\circ$ and the Kolmogorov time scale, it is possible to compare the orientation distribution of different ramified particles settling in different flow fields. Fig. 2.3 shows the orientation distribution of triads and fibers settling at the two Re_λ. It is interesting to note that by defining an empirical S_F based on the Kolmogorov time scale and $\tau_{sed,45^\circ}$, one may compare the average variance of deviations away from horizontal for different geometries. All the expected asymptotes and transitions are successfully captured in Fig. 2.3. As one might expect the transition from isotropic to horizontal alignment tends to start at $S_F \sim O(1)$.

To conclude, if we define the order parameter $\mathcal{P}$,as the average variance of deviation of arms from horizontal, we have the following S_F^{-2} relationships for fibers,

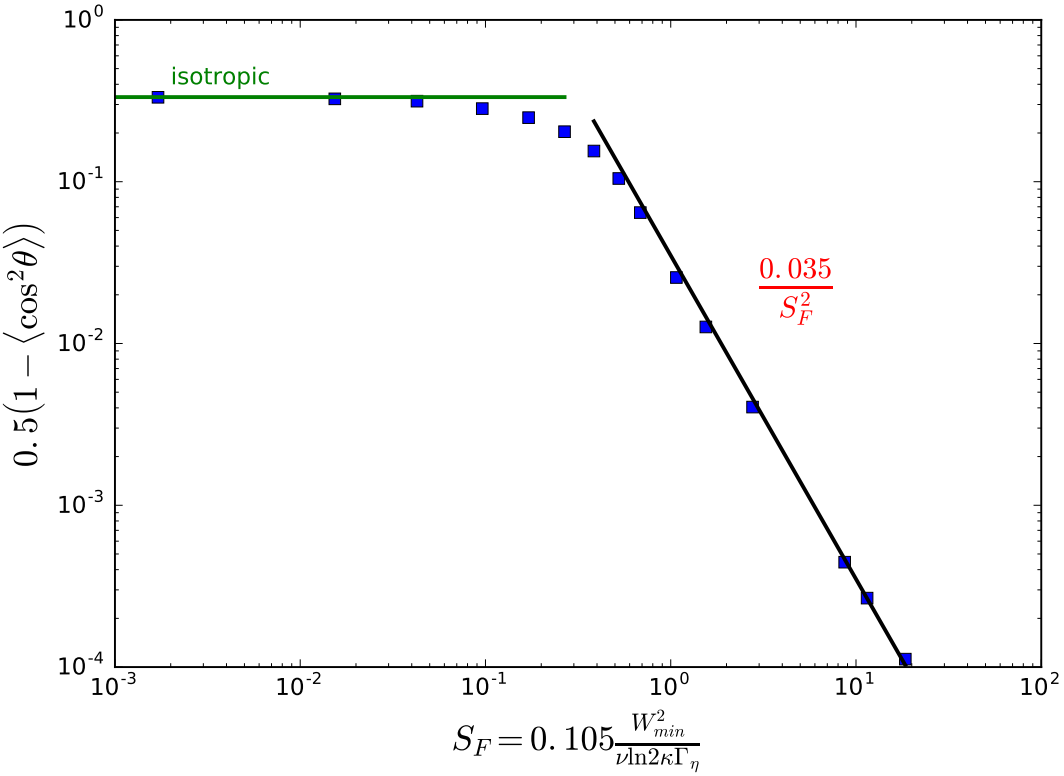

Figure 2.2: Orientation variance of small triads as a function of settling factor, S_F. The squares correspond to simulations and the lines are asymptotes derived in the low and high S_F limits.

triads, and disks:

$$\mathcal{P}_{fiber} = \langle \cos^2\theta \rangle \approx \frac{0.033}{S_F^2} \tag{2.45}$$

$$\mathcal{P}_{triad} = 0.50\left(1 - \langle\theta^2\rangle\right) \approx \frac{0.035}{S_F^2} \tag{2.46}$$

$$\mathcal{P}_{disks} \approx \frac{0.042}{S_F^2} \tag{2.47}$$

A similar analytical analysis for disks provided by our collaborator Prof. Roy gives the order parameter of disks mentioned above for comparison, details of this derivation has been consciously omitted in this thesis. It is interesting to

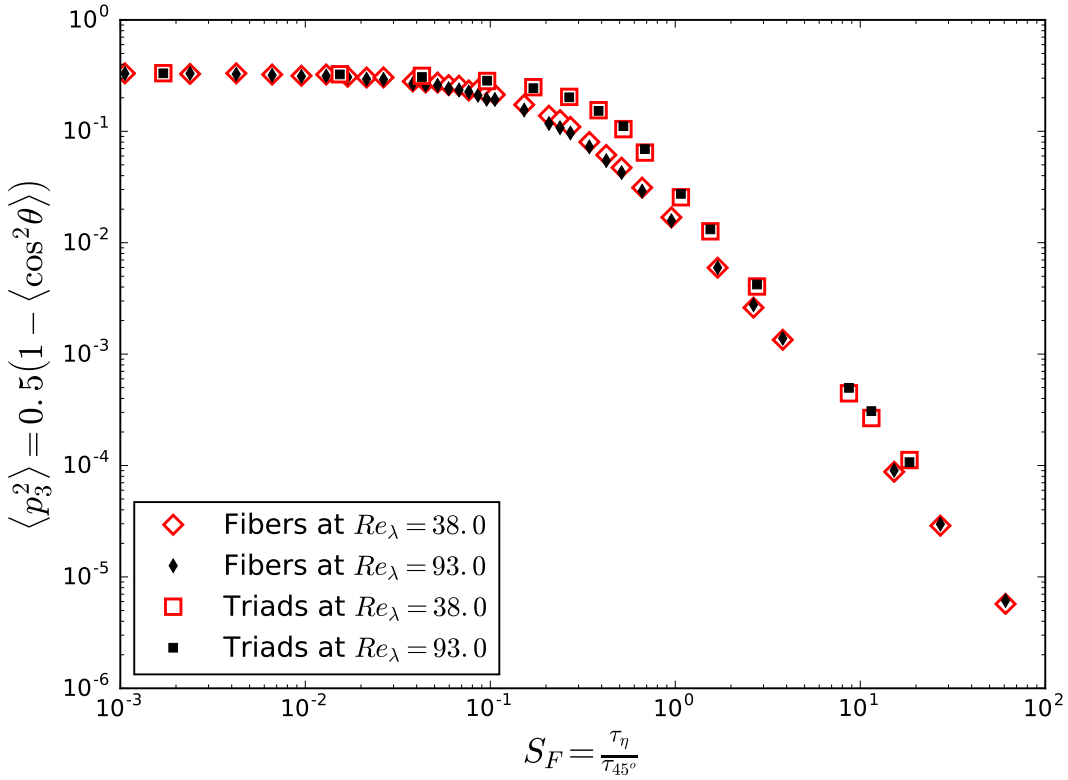

Figure 2.3: Orientation variance of ramified particles as a function of the empirical settling factor, S_F.

note that the ramified particle shows a similar S_F^{-2} behavior to fibers and disks. The theoretical coefficients for triads and fibers agree and is approximately the same in simulations if there is a complete de-correlation of particle orientation and velocity gradient. However, as can be seen in Fig. 2.3 and 2.2, for fibers the theoretical asymptote needs a correction to account for this correlation of particle orientation and velocity gradient in our simulations using Lagrangian stochastic model of Girimaji and Pope [7]. This is the reason for fiber asymptote appearing different from the triad asymptote at high S_F limit.

2.5 Comparison to experiments

Experiments have been carried out to observe the sedimentation of ramified particles in homogeneous isotropic turbulence at the Voth group in Wesleyan University. Our simulations and theory have been compared to the experimental findings of Stefan Kramel [13]. In these experiments, two different sized triad particles were studied, both of larger length scales than the Kolmogorov length η. The experiments involve stronger turbulence, $Re_\lambda \sim O(100)$ and fluid inertia effects that cannot be described as weak $O(Re_\ell)$ torques like we do in our theory and simulations. In Table 2.1, we report some of the experimental details of Stefan's work to highlight the realistic range of parameters one deals with in experiments [13]. The ramified particles in the experiment were fabricated using 3D printing technology and can be extended to create more complicated geometries in a similar way. The motivation for choosing triads is that they capture the particle symmetries of a disk and in Stokes flow they are known to exhibit similar rotational dynamics. However, we expect the fluid inertia to be of consequence and lead to differences in the orientational dynamics of triads and disks.

In the experiments, the particles settle in a vertical fluid column that has a homogeneous isotropic turbulence. The particle are heavy and have a relative density $\Delta\rho \approx 0.146$ with respect to the fluid ($\Delta\rho = \frac{\rho_p - \rho_f}{\rho_f}$), allowing them to settle due to gravity. Two triads of arm lengths $L = 9mm$ and $18mm$ were fabricated, referred to here as small and large triads respectively, and have an aspect ratio of $\kappa = 20$. In a quiescent flow of viscosity $\nu \approx 0.91 mm^2 s^{-1}$, the small and large triads have a minimum velocity W_{min}, at horizontal orientation, of $23.2mm\ s^{-1}$ and $36.8mm\ s^{-1}$ respectively. The triads experience Re_D and Re_ℓ in the range of

20 – 40 and 200 – 400 respectively. The turbulence intensity is defined as the ratio of rms velocity fluctuation in the direction of flow to mean flow in the channel. Another parameter useful to quantify turbulence is the corresponding dissipation rates $\langle\epsilon\rangle$, given in Table 2.1 for different flows in the channel.

In the experiments, we have $Re_\ell > 1$ and as a result, the empirical definition of

Small Triads					Large Triads				
Turb. Intensity	$\langle\epsilon\rangle$ $mm^2\ s^{-3}$	Re_λ	η mm	τ_η s	Turb. Intensity	$\langle\epsilon\rangle$ $mm^2\ s^{-3}$	Re_λ	η mm	τ_η s
0.07	0.04	29	2.16	5.11	0.07	0.25	36	1.32	1.91
0.21	0.75	91	1.00	1.12	0.10	0.30	56	1.26	1.77
0.39	9.50	141	0.53	0.31	0.29	7.50	102	0.56	0.35
0.62	30	162	0.39	0.18	0.28	30	153	0.40	0.17
0.91	50	192	0.35	0.14	0.37	50	162	0.35	0.14
1.06	60	194	0.33	0.13	0.95	180	200	0.25	0.07

Table 2.1: Relevant experimental details reported from the work of Stefan Kramel [13]. The small and large triads are made of arms of lengths $9mm$ and $18mm$ respectively. The arms have an aspect ratio of $\kappa = 20$. Further details may be found in the thesis mentioned.

S_F is handy as it is easier to determine the rotation rate $\dot{\boldsymbol{p}}$ at an angle of $\theta = 45°$. Since the particles are larger than Kolmogorov length scales, in experiments one must also slightly modify the definition of S_F to account for the eddies that contribute the most to turbulent randomization of the triad. This gives a slightly different definition of S_F to be,

$$S_F = \frac{\tau_L}{T_{sed,45°}} = \tau_L \langle |\dot{\boldsymbol{p}}_{sed,45°}| \rangle \tag{2.48}$$

$$T_{sed,45°} = \frac{1}{\langle |\dot{\boldsymbol{p}}_{sed,45°}| \rangle} \tag{2.49}$$

The measured inverse rotation rate $T_{sed,45°}$ for small and large triads were measured to be $(1.7 \pm 0.1)\ s$ and $(1.9 \pm 0.1)\ s$, respectively.

This experimental S_F corresponds to the empirical settling parameter we used in theory, $S_F = \tau_\eta/\tau_{sed,45^\circ}$. Thus we are able to compare the triad simulations and theory to experiments. Fig 2.4, shows this comparison between experiments

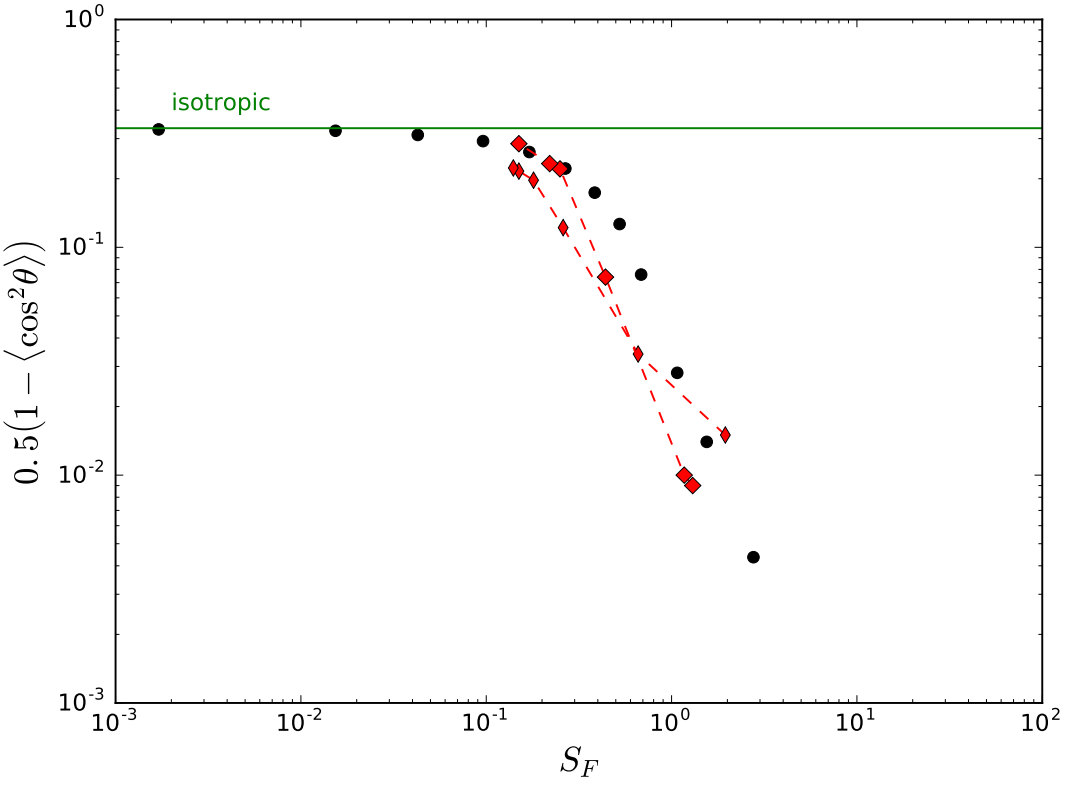

Figure 2.4: Comparison of experiments and simulations showing orientation variance of triads as a function of the empirical settling factor, S_F. The large and small diamonds correspond to larger and smaller triad particles in the experiments, of arm lengths 18*mm* and 9*mm* respectively. The arms have an aspect ratio of $\kappa = 20$. The simulations at different horizontal velocities are shown as black circles. S_F in simulations is based of inverse rotation rate of triads at $\theta = 45^\circ$ and Kolmogorov shear rate Γ_η, similar to the approach used in experiments.

and simulations. It must be remembered that the model is a simple description of triad as three fibers connected and constrained to perform rigid body

dynamics without any arm to arm interactions. In the experiments, this is most definitely not true, as there is going to be interaction between arms. While the effects of such interactions are not thought of in this work, we expect them to be critical and it would warrant DNS simulations that allow for two-way coupled fiber-fluid interactions. However, it is commendable that we observe agreement between the different results while capturing the important trends qualitatively and quantitatively to some extent. It is also interesting to note that by defining the settling parameter in terms of two time scales based of particle rotation due to turbulence and fluid inertia, we have developed a robust settling parameter S_F and observe a S_F^{-2} asymptote at the rapid settling limit across different flows and studies. The slight mismatch that we see in Fig. 2.4 between the experiments and simulations/theory may be attributed to the simplicity of the model and disregard of any arm to arm interactions.

CHAPTER 3

CONCLUSION

The objective of this work was to develop a model for ramified particles and simulate their orientation dynamics using a stochastic model of turbulence. In this regard, a simple but robust particle model exploiting the high aspect ratio of fibers using Slender Body theory [1] was developed. The fibers we have simulated have an aspect ratio of $\kappa = 20$, same as the particles in the experiments of Stefan Kramel [13] that we compare to in section 2.5. This is a high enough aspect ratio to use Slender Body theory. Our model is a leading order approximation of the different torques experiences by fibers while settling in turbulence. To gather more information surrounding the sedimentation of fibers in turbulence, one must perform Direct Numerical Simulations (DNS). While many DNS related works have been performed in the past, there is a lack of simulations involving two-way coupled interaction of fluid and fibers. Fluid inertia is critical to fiber orientation dynamics and appears as a result of two-way coupled interaction between fiber and fluid. For example, the broadside alignment of high aspect ratio particles that is responsible for breaking the degeneracy of turbulent randomization is due to fluid inertia. In a DNS simulation, these effects may be captured by considering the effects of fiber on fluid and vice versa, commonly referred to as two-way interactions. However, including two-way coupling in DNS simulations is not straightforward and not successfully implemented. There have been some simulations that have attempted to tackle this conundrum by considering situations involving either turbulence or fluid inertia effects. Shin and Koch [20] have, for example, simulated neutrally buoyant fibers in turbulence. This assumption avoids any need to include fluid inertia, as the drag on fiber is necessary for creating any fluid inertial torque or

coupling of fluid and particle phase interaction. Similarly, works [21, 22] that do consider fluid inertia and its effects on fiber dynamics have chosen to ignore the effects of turbulence in their calculations. Due to a lack of DNS solvers and the ease of using a stochastic model over solving the entire Navier-Stokes equation, this approach of including the fluid inertia effects in the particle model has been convenient and useful. However, it is necessary to remind that such an approximation is only valid when we are considering weak fluid inertia $O(Re_\ell)$. We have applied this model to fibers and triads to understand the utility of our approach. While fibers remain the basic unit for application of this approach, by extending this model to triads, we have shown how one may be able to model complicated ramified particles as fibers connected together. This in a way corresponds to the approach adapted by experimentalists to fabricate shapes using 3D printing where rods are connected together.

Girimaji and Pope [7] models homogeneous isotropic turbulence (HIT) turbulence as a stochastic velocity gradient using Uhlenbeck-Ornstein process. The salient feature of this model is that it captures the non linear terms in the Navier-Stokes equation, responsible for inertial effects, exactly. It uses the temporal diffusion equation of log-normal pseudo-dissipation of Chen and Pope [17] as a starting point to develop a stochastic differential equation of velocity gradient tensor. The model is then tuned and constrained to match the pseudo-dissipation distribution and higher velocity gradient moments observed in the DNS simulations of Yeung and Pope [26]. As a result, the model captures the correlations observed, in DNS, between the fluid vorticity and shear. This coupling of shear and vorticity is important for successful simulation of fiber orientation dynamics.

Since, the model captures only the leading order effects of fluid inertia, it is im-

portant to realize that our simulations are a best representation of weak inertia $Re_\ell = U\ell/\nu \ll 1$ and weak turbulence $G = \ell\Gamma_\eta/U \ll 1$, and for sub-Kolmogorov $\ell < \eta$ particles. However, we consider the entire spectrum of relative settling rates through the settling parameter S_F. Settling parameter ($S_F \equiv Re_\ell/G$) is the ratio of response time scales to fluid inertia τ_{sed} and turbulence τ_η, the two important contributions to orientation dynamics of high aspect ratio particles.

Through our simulations and theory for fibers in sections 2.3 and 2.3.1, we have identified the important regions of fiber orientation depending on the relative influence of fluid inertia and turbulence. At low S_F, we observe from Fig. 2.1 that the fiber orientation is influenced by the turbulence strongly, and as a result, the particle responds to the stochastic velocity gradient relatively quickly while following a Lagrangian trajectory. This results in an isotropic distribution of the particle orientation. As the particle settling velocity increases, there is a larger influence of fluid inertia leading to a horizontal alignment of the fibers. This appears as an asymptotic decrease in the particle orientation variance in Fig. 2.1. This decrease in variance has a S_F^{-2} behaviour at rapid settling limit, as expected from theory. At this regime, the particle responds quickly to the inertial torque, resisting deviations away from the horizontal due to turbulence. However, for fibers, this appears as a resistance only in the 3-component of fiber orientation, and as a result, the 1, 2 components continue to respond to turbulence time scales. This leads to a partial correlation of particle orientation and velocity gradient in our simulations. In our theory, we assume the particle orientation to completely de-correlate from the fluid flow at the rapid settling limit. For fibers, we add a factor of correlation to our theoretical asymptote, as shown in Eq. 2.32, to compare to simulations in Fig. 2.1.

We have extended this idea from fibers to triads in section 2.4, where we model

the triad as three co-planar fibers constrained by rigid body dynamics. While this is a rudimentary model that neglects any arm to arm interactions, this model captures the essential features and influences of the two important time scales involved. By defining a settling parameter as the ratio of two time scales τ_{sed} and τ_{η}, like we did for fibers, we have simulated the orientation distribution of triads settling in turbulence as shown in Fig. 2.2. Like in the case for fibers, the simulations capture the sub-Kolmogorov dynamics at weak inertia and weak turbulence but for different relative strengths through S_F. We determine the time scale of response to fluid inertia τ_{sed} as an inverse rotation rate at $\theta = 45^{\circ}$ by simulating the rotation due to inertia torque in a quiescent flow. Using the empirical definition of S_F, we have defined a general settling parameter that may be used to compare orientation dynamics across particles and Re_{λ}. In Fig. 2.3, we compare our simulations of fibers and triads performed at $Re_{\lambda} = 38$ and 93. We see, that this definition of S_F helps in identifying a universal power-law relation of asymptote at the rapid settling limit. It is commendable that our simple model is useful in generating simulations and theoretical asymptotes that are valid across different flow and particle parameters as shown in Fig. 2.3. Finally, we compare our simulations and theory to the experimental results of Kramel [13] in section 2.5. As expected, the experiments are not restricted by the assumptions made in theory or simulations. The particles are no longer sub-Kolmogorov and there is more than just leading order effects captured. However, by ensuring a similar definition of S_F is used, we are able to compare our simulations to the experiments in Fig. 2.4. As can be seen, our simulations capture the trends and transitions seen in experiments well. The difference in rapid settling asymptote coefficients observed may be attributed to the limitations and assumptions in our model. For example, the experiments contain

particles, where the arms are not independent of each others' influence. We believe these arm interactions and other higher order effects of fluid inertia might be responsible for this difference. To verify these details through simulations, one must perform DNS of fibers and triads. It must be also reminded that we have used a Lagrangian model of turbulence. While this may be easily justified at the low settling limit $S_F \ll 1$, we argue that at $S_F \gg 1$, the particle responds to fluid inertia quickly and as a result, the frame of reference we choose for turbulent velocity gradient is inconsequential. However, as observed from our fiber simulation and theory comparison in Fig. 2.1, a particle frame model of velocity gradient that involves the particle settling rates is necessary. Also, at $S_F \sim O(1)$ these arguments are no longer valid, and one must use a particle frame model of turbulence. But it is important to note that our approach is still capable of capturing the trends observed in experiments at all S_F.

To conclude, we would like to reiterate that our model is a simple description of high aspect ratio particles, capturing the important contributions to their dynamics due to turbulence and fluid inertia. The model is valid for sub-Kolmogorov particles ($L < \eta$) settling under weak inertia and weak turbulence. We have, however, through our simulations and theory captured the salient features of particle orientation dynamics, and defined a settling parameter S_F in the process, that is useful in understanding the orientation distribution of different ramified particles across various flow parameters. We have finally identified a S_F^{-2} behavior at rapid settling limit that appears to be universal for high aspect ratio particles and derived expressions for the same. This work would hopefully serve as a source of motivation for DNS of fibers and other high-aspect ratio particles in turbulence.

BIBLIOGRAPHY

[1] GK Batchelor. Slender-body theory for particles of arbitrary cross-section in stokes flow. *Journal of Fluid Mechanics*, 44(3):419–440, 1970.

[2] Brett K Brunk, Donald L Koch, and Leonard W Lion. Turbulent coagulation of colloidal particles. *Journal of Fluid Mechanics*, 364:81–113, 1998.

[3] Laurent Chevillard and Charles Meneveau. Lagrangian dynamics and statistical geometric structure of turbulence. *Physical review letters*, 97(17):174501, 2006.

[4] Laurent Chevillard and Charles Meneveau. Intermittency and universality in a lagrangian model of velocity gradients in three-dimensional turbulence. *Comptes Rendus Mécanique*, 335(4):187–193, 2007.

[5] HR Cho, JV Iribarne, and WG Richards. On the orientation of ice crystals in a cumulonimbus cloud. *Journal of the Atmospheric Sciences*, 38(5):1111–1114, 1981.

[6] Roland Clift, John R Grace, and Martin E Weber. *Bubbles, drops, and particles*. Courier Corporation, 2005.

[7] SS Girimaji and SB Pope. A diffusion model for velocity gradients in turbulence. *Physics of Fluids A: Fluid Dynamics*, 2(2):242–256, 1990.

[8] K Gustavsson, J Jucha, A Naso, E Lévêque, A Pumir, and B Mehlig. Statistical model for the orientation of nonspherical particles settling in turbulence. *Physical review letters*, 119(25):254501, 2017.

[9] Bardia Hejazi, Bernhard Mehlig, and Greg A Voth. Emergent scar lines in chaotic advection of passive directors. *Physical Review Fluids*, 2(12):124501, 2017.

[10] Kimberly H Henthorn, Kinam Park, and Jennifer S Curtis. Measurement and prediction of pressure drop in pneumatic conveying: Effect of particle characteristics, mass loading, and reynolds number. *Industrial & engineering chemistry research*, 44(14):5090–5098, 2005.

[11] RE Khayat and RG Cox. Inertia effects on the motion of long slender bodies. *Journal of Fluid Mechanics*, 209:435–462, 1989.

[12] James D Klett. Orientation model for particles in turbulence. *Journal of the atmospheric sciences*, 52(12):2276–2285, 1995.

[13] Stefan Kramel. Non-spherical particle dynamics in turbulence. 2018.

[14] Stefan Kramel, Greg A Voth, Saskia Tympel, and Federico Toschi. Preferential rotation of chiral dipoles in isotropic turbulence. *Physical review letters*, 117(15):154501, 2016.

[15] Vincent Noel and Kenneth Sassen. Study of planar ice crystal orientations in ice clouds from scanning polarization lidar observations. *Journal of Applied Meteorology*, 44(5):653–664, 2005.

[16] Shima Parsa, Enrico Calzavarini, Federico Toschi, and Greg A Voth. Rotation rate of rods in turbulent fluid flow. *Physical Review Letters*, 109(13):134501, 2012.

[17] SB Pope and YL Chen. The velocity-dissipation probability density function model for turbulent flows. *Physics of Fluids A: Fluid Dynamics*, 2(8):1437–1449, 1990.

[18] Alain Pumir and Michael Wilkinson. Orientation statistics of small particles in turbulence. *New journal of physics*, 13(9):093030, 2011.

[19] Kenneth Sassen, Vinay Kumar Kayetha, and Jiang Zhu. Ice cloud depolarization for nadir and off-nadir calipso measurements. *Geophysical Research Letters*, 39(20), 2012.

[20] Mansoo Shin and Donald L Koch. Rotational and translational dispersion of fibres in isotropic turbulent flows. *Journal of Fluid Mechanics*, 540:143–173, 2005.

[21] Mansoo Shin, Donald L Koch, and Ganesh Subramanian. A pseudospectral method to evaluate the fluid velocity produced by an array of translating slender fibers. *Physics of Fluids*, 18(6):063301, 2006.

[22] Mansoo Shin, Donald L Koch, and Ganesh Subramanian. Structure and dynamics of dilute suspensions of finite-reynolds-number settling fibers. *Physics of Fluids*, 21(12):123304, 2009.

[23] Greg A Voth and Alfredo Soldati. Anisotropic particles in turbulence. *Annual Review of Fluid Mechanics*, 49:249–276, 2017.

[24] CD Westbrook, AJ Illingworth, EJ O'Connor, and RJ Hogan. Doppler lidar measurements of oriented planar ice crystals falling from supercooled and glaciated layer clouds. *Quarterly Journal of the Royal Meteorological Society*, 136(646):260–276, 2010.

[25] Michael Wilkinson, Vlad Bezuglyy, and Bernhard Mehlig. Fingerprints of random flows? *Physics of Fluids*, 21(4):043304, 2009.

[26] PK Yeung and SB Pope. Lagrangian statistics from direct numerical simulations of isotropic turbulence. *Journal of Fluid Mechanics*, 207:531–586, 1989.

[27] Lihao Zhao and Helge I Andersson. Why spheroids orient preferentially in near-wall turbulence. *Journal of Fluid Mechanics*, 807:221–234, 2016.

[28] Lihao Zhao, Niranjan Reddy Challabotla, Helge I Andersson, and Evan A Variano. Rotation of nonspherical particles in turbulent channel flow. *Physical review letters*, 115(24):244501, 2015.